Separation of the reservoir and wave pressure and velocity from measurements at an arbitrary location in arteries

J Aguado-Sierra[1], **J Alastruey**[1,2], **J-J Wang**[3], **N Hadjiloizou**[4], **J Davies**[4], and **K H Parker**[1*]
[1]Department of Bioengineering, Imperial College, London, UK
[2]Department of Aeronautics, Imperial College, London, UK
[3]University of Calgary, Calgary, Canada
[4]International Centre for Circulatory Health, Imperial College, London, UK

The manuscript was received on 25 March 2007 and was accepted after revision for publication on 29 November 2007.

DOI: 10.1243/09544119JEIM315

Abstract: Previous studies based on measurements made in the ascending aorta have demonstrated that it can be useful to separate the arterial pressure P into a reservoir pressure $\bar{P}$ generated by the windkessel effect and a wave pressure p generated by the arterial waves: $P = \bar{P} + p$. The separation in these studies was relatively straightforward since the flow into the arterial system was measured. In this study the idea is extended to measurements of pressure and velocity at sites distal to the aortic root where flow into the arterial system is not known. $\bar{P}$ is calculated from P at an arbitrary location in a large artery by fitting the pressure fall-off in diastole to an exponential function and assuming that p is proportional to the flow into the arterial system. A local reservoir velocity $\bar{U}$ that is proportional to $\bar{P}$ is also defined. The separation algorithm is applied to *in vivo* human and canine data and to numerical data generated using a one-dimensional model of pulse wave propagation in the larger conduit arteries. The results show that the proposed algorithm is reasonably robust, allowing for the separation of the measured pressure and velocity into reservoir and wave pressures and velocities. Application to data measured simultaneously in the aorta of the dog shows that the reservoir pressure is fairly uniform along the aorta, a test of self-consistency of the assumptions leading to the algorithm. Application to data generated with a validated numerical model indicates that the parameters derived by fitting the pressure data are close to the known values which were used to generate the numerical data. Finally, application to data measured in the human thoracic aorta indicates the potential usefulness of the separation.

Keywords: reservoir pressure, wave pressure, reservoir velocity, wave velocity, arteries, windkessel model, one-dimensional model

1 INTRODUCTION

The mechanics generating the characteristic shape of the arterial pressure waveform measured in normal subjects were first described quantitatively by Frank [**1**] in 1899 using an air chamber or *windkessel* model. This model highlights the importance of the arterial compliance in transforming the discontinuous cardiac output into a more steady pressure and flow in the arteries and microcirculation. Indeed, if arteries were rigid, pressure changes would occur at the same time everywhere in the system, and the blood flow into the microcirculation would be instantaneously equal to the blood flow out of the ventricle, leading to zero blood flow during diastole.

The windkessel model excels in explaining the diastolic part of the pressure waveform, but it fails to reproduce the systolic part because pressure changes are assumed to occur synchronously throughout the arteries without accounting for the wave nature of pulse wave propagation, as also

Corresponding author: Department of Bioengineering, Royal School of Mines Building, Imperial College, London, SW7 2AZ, UK. email: k.parker@ic.ac.uk

noticed by Frank [**2**]. The basic equations describing flow in the flexible arteries were first introduced by Euler [**3**] in 1775, who derived the one-dimensional partial differential equations expressing the conservation of mass and momentum for inviscid flow. These equations can be solved in the time domain using the method of characteristics developed by Riemann [**4**] or in the frequency domain using Fourier analysis [**5**]. Both solutions show that pressure and flow waveforms can be understood as forward-running waves originating at the left ventricle, and backward or reflected waves [**6**, **7**].

Although forward and backward waves are able to explain changes in pressure and flow waveforms through the arterial system during systole, including their alterations due to ageing, vascular diseases, and invasive clinical procedures, they fail to explain pressure and flow waveforms during diastole. Indeed, the equal and opposite waves predicted during diastole are difficult to explain physiologically at the time when the aortic valve is closed. Wang *et al.* [**8**] proposed a unifying windkessel–wave theory that provides a suitable explanation of central aortic pressure and flow waveforms during the whole cardiac cycle. In this work, the central aortic pressure was decomposed into the sum of a time-varying reservoir pressure $\bar{P}(t)$, governed by Frank's windkessel model, and a wave pressure $p(x, t)$ that varies in time t and with the distance x along the arteries. The notation in the work of Wang *et al.* [**8**, **9**] is different from that used here. They referred to the 'reservoir' pressure as the 'windkessel' pressure and the 'wave' pressure as the 'excess' pressure. Apart from this difference in names, the definitions are the same. This decomposition shows a striking similitude between measured wave pressure and central aortic flow during the whole cardiac cycle (see Fig. 5A in reference [**8**]). The separation of measured pressure into a reservoir pressure and a wave pressure has also been applied to measurements in the central venous system with equally striking results [**9**].

The Wang *et al.* model provides a suitable explanation of the mechanics of pulse wave propagation, although it can only be applied to measurements made in the ascending aorta when the measured flow is equal to the flow into the arterial system. In this work, a new algorithm, based on empirical hypotheses is proposed to determine the reservoir pressure from pressure measurements alone at an arbitrary arterial location. Furthermore, a decomposition of measured flow at the same location into a reservoir and a wave component that are directly related to their pressure counterparts is proposed. The implications of this new separation technique are explored using *in vivo* and numerical data.

Note that the three-element windkessel model proposed by Westerhof *et al.* [**10**] and widely used for arterial modelling [**11**] is an alternative way to express the reservoir component of the model that is proposed here. However, the present authors are unaware of any model that uses the electrical analogy and is equivalent to the hypothesis on combined reservoir and wave components.

2 METHODOLOGY

2.1 Previous work on the calculation of the reservoir pressure

The work by Wang *et al.* [**8**] on the reservoir–wave separation calculated the reservoir pressure $\bar{P}$, using the pressure P_{in} and flow Q_{in} measured at the inlet to the arterial system, neglecting the flow through the coronary system. This method solves the conservation of mass in the arterial system according to

$$\frac{\mathrm{d}V}{\mathrm{d}t} = Q_{\text{in}} - Q_{\text{out}} \tag{1}$$

where V is the volume of the arterial system and Q_{out} is the flow out of the arteries through the microcirculation, by assuming that, first, the compliance of the whole arterial tree, which is given by $C = \mathrm{d}V/\mathrm{d}P$, is constant and, second, the flow through the microcirculation can be written in terms of a simple resistive relationship $Q_{\text{out}} = (\bar{P} - P_{\infty})/R$, where R is the effective resistance of the peripheral systemic circulation and P_{∞} is the pressure, assumed to be constant, at which flow through the microcirculation is zero. It is note that P_{∞} is not necessarily the venous pressure but could be related to the tissue pressure surrounding the microcirculation.

Using the above two assumptions, equation (1) can be written as

$$\frac{\mathrm{d}\bar{P}}{\mathrm{d}t} + \frac{\bar{P} - P_{\infty}}{RC} = \frac{Q_{\text{in}}}{C} \tag{2}$$

This equation can be solved by multiplying by the integrating factor $\mathrm{e}^{t/\tau}(\tau \equiv RC)$ with the result

$$\bar{P} - P_{\infty} = \left(\bar{P}_0 - P_{\infty}\right) \mathrm{e}^{-t/\tau} + \frac{\mathrm{e}^{-t/\tau}}{C} \int_0^t Q_{\text{in}}(t')\, \mathrm{e}^{t'/\tau}\, \mathrm{d}t' \tag{3}$$

where $\bar{P}_0$ corresponds to the pressure at the onset of

the ejection. During diastole, where the inflow Q_{in} is zero, equation (3) is used to fit P_∞ and the time constant τ to the experimentally measured pressure P_{in}. Approximately the last two thirds of diastole of P_{in} is used, when wave activity is believed to be at a minimum. An estimate of the resistance is calculated as $R = <P_{in}>/<Q_{in}>$, where $<P_{in}>$ and $<Q_{in}>$ are the time-averaged pressure and time-averaged flow respectively over the cardiac cycle at the ascending aorta.

The wave nature of the system derives from the one-dimensional theory of flow in elastic tubes. A propagating wave is a disturbance generated by an excess pressure p over an undisturbed pressure $\bar{P}$ [**12**]. The measured aortic pressure waveform was defined as having a reservoir component and wave component as $P_{in} = \bar{P} + p$.

2.2 Extension of the theory to measurements at an arbitrary location

An extension of the previous theory is proposed on the basis of the following observations.

1. The pressure waveform decay measured at different locations in the arterial system is very similar in diastole. For example, the pressure measured in the carotid arteries is very similar to the pressure waveform measured in the ascending aorta, although the flow waveforms are qualitatively different (see, for instance, Fig. 4 in reference [**13**]). Recent measurements in the coronary arteries also show pressure waveforms that are very similar to those measured in the aorta in the same subject [**14**].
2. When the wave pressure in the ascending aorta (the difference between the measured pressure and the reservoir pressure calculated from the measured flow) is plotted against the measured flow waveform, an almost straight line is obtained (see Fig. 2 in reference [**8**]). This indicates that the flow in the ascending aorta is dominated by forward-travelling waves. Thus, arterial bifurcations should be close to well matched for forward waves and, hence, the wave pressure measured at any aortic location is approximately proportional to the cardiac output. Observation of well-matched bifurcations for forward waves in humans has been reported in reference [**15**].

If both of these observations are true, then it should be possible to determine a reservoir pressure $\bar{P}(t)$ from a pressure waveform $P(x, t)$ measured at an arbitrary location in the arterial tree. Assuming that $\bar{P}$ is determined from the conservation of mass described by equation (2) using the same assumptions about the compliance of the whole arterial system and the resistive nature of flow through the microcirculation, the last term of this equation can be written in terms of $\bar{P}$. By the second observation (assumption) above, Q_{in} can be approximated as being proportional to the difference between P and $\bar{P}$ that it is required to calculate. This can be written simply as $Q_{in} = \gamma(P - \bar{P})$, where γ is a constant which will depend upon a number of factors, such as the local wave speed and cross-sectional area at the root of the aorta. Therefore, equation (2) leads to

$$\frac{d\bar{P}}{dt} = a(P - \bar{P}) - b(\bar{P} - P_\infty) \tag{4}$$

where $a = \gamma/C$ and $b = 1/\tau$ are the rate constants of the system with the units s^{-1}.

Under normal conditions, $Q_{in} = 0$ for $T_N \leqslant t \leqslant T$, where T_N is the time when the aortic valve shuts at the end of systole and T is the time when the heart beat ends. During this period of time, equation (4) reduces to

$$\frac{d\bar{P}}{dt} = -b(\bar{P} - P_\infty), \quad T_N \leqslant t \leqslant T \tag{5}$$

It is considered that T_N corresponds to the time when the dicrotic notch appears in P. In the case of a pressure waveform without a clearly marked notch, T_N is taken to be the time of the first zero crossing of the second derivative of pressure at the end of systole. The general solution of equation (5) is

$$\bar{P} - P_\infty = [\bar{P}(T_N) - P_\infty]e^{-b(t - T_N)}, \quad T_N \leqslant t \leqslant T \tag{6}$$

Considering that the reservoir effect is the main driver of the exponential pressure fall-off in diastole, and wave activity is minimum, the constant parameters $\bar{P}(T_N)$, P_∞, and b can be estimated by fitting them to experimental data P using equation (6). It is noted that data were non-dimensionalized for better performance of the unconstrained non-linear optimization algorithm selected. The MATLAB routine fminsearch was used with non-dimensionalised initial conditions equivalent to $\bar{P}(T_N) = P(T_N)$ and $b = 1\,s^{-1}$, and a tolerance of $1\,e^{-12}$. This function uses the simplex search method described in reference [**16**]. It is assumed that $P_\infty = 0$ for experimental data. There is a suggestion [**9**], however, that P_∞ should not be the venous pressure, but an intermediate pressure associated with the waterfall or the mean circulatory pressure. In the numerical

model, $P_\infty = 432.6\,\text{Pa}$, which corresponds to the venous pressure previously established as a boundary condition.

During systole, equation (4) can be solved explicitly using the integration factor $e^{(a+b)t}$, to give

$$\bar{P} = \frac{b}{a+b}P_\infty + e^{-(a+b)t} \times \left[\int_0^t aP(t')\, e^{(a+b)t'}\, dt' + \bar{P}_0 - \frac{b}{a+b}P_\infty\right], \quad 0 \leqslant t \leqslant T_N \tag{7}$$

where $\bar{P}_0$ corresponds to the start point of the onset of P, since little wave activity is expected at the end of the previous beat. Note that the second observation needs only to be true during the systolic period $0 \leqslant t \leqslant T_N$. To determine the unknown parameter a, continuity of $\bar{P}$ at $t = T_N$ is enforced, which yields

$$\bar{P}(T_N) = \frac{b}{a+b}P_\infty + e^{-(a+b)T_N} \times \left[\int_0^{T_N} aP(t')\, e^{(a+b)t'}\, dt' + \bar{P}_0 - \frac{b}{a+b}P_\infty\right] \tag{8}$$

The parameter a is fitted from experimental data using the fminsearch MATLAB routine described above, with non-dimensionalized data, an initial value equivalent to $10\,\text{s}^{-1}$, and a tolerance of $1\,e^{-12}$. $\bar{P}$ is determined for the entire period from equations (6) and (7).

2.3 Extension to reservoir velocity

The velocity $\bar{U}$ due to the reservoir pressure is assumed to be zero in the Wang *et al.* [**8**] model. This is a good assumption in the ascending aorta, as shown by experimental measurements where the velocity is invariably zero during the later part of diastole. However, it should not be true in more distal vessels. It is now assumed that both the pressure and the velocity can be resolved into a reservoir and a wave component: $P = \bar{P} + p$ and $U = \bar{U} + u$. However, while $\bar{P}$ is only time varying, $\bar{U}$ also depends upon position, i.e. $\bar{U}(x, t)$.

To determine $\bar{U}$, it is established that it has to be directly proportional to $P - P_\infty$ at the end of diastole when the reservoir effect is dominant and, hence, wave activity is expected to be minimal. This can be written as

$$\bar{U} = \frac{P - P_\infty}{\bar{R}} \tag{9}$$

where $\bar{R}$ is the effective resistance of the vessels downstream of the measurement site. Note that the *PU*-loop proposed in reference [**17**] states there is a linear relationship between P and U when only unidirectional waves are present. The slope is equal to $\pm\rho c$, where ρ is the blood density, c is the pulse wave speed, and the sign indicates the direction of the waves.

The quest for the exact portion with the best linear relationship of P and U in diastole was implemented using a Bayesian statistics-based method for linearity testing, programmed using MATLAB. However, for some cases, particularly at high heart rates, the linear portion is difficult to identify, since waves may still be present. For such cases, and to ensure robustness and applicability of the algorithm to cases in which U is not available or data are noisy, $\bar{R}$ is determined as $\bar{R} = (\langle P\rangle - P_\infty)/\langle U\rangle$, where $\langle P\rangle$ and $\langle U\rangle$ are the time-averaged pressure and time-averaged velocity respectively at $T_N \leqslant t \leqslant T$.

Once $\bar{R}$ has been determined, $\bar{U}$ can be calculated at any time $0 \leqslant t \leqslant T$ as

$$\bar{U} = \frac{\bar{P} - P_\infty}{\bar{R}} \tag{10}$$

The wave velocity is then $u = U - \bar{U}$, which will generally be non-zero except at the root of the aorta during diastole. This velocity $\bar{U}$ is equal to the velocity due to the reservoir pressure if the compliance downstream of the measuring site is negligible.

3 RESULTS

3.1 *In vivo* data

Simultaneous P and U measurements from dogs were provided by Wang *et al.* [**8**] for analysis. Measurements were performed at four different sites: the ascending aorta, the aortic arch, 11 cm after the aortic valve, the thoracic aorta, at 24 cm, and abdominal aorta, at 45 cm. The areas were calculated as $2.6\,\text{cm}^2$, $1.5\,\text{cm}^2$, $1.5\,\text{cm}^2$, and $0.5\,\text{cm}^2$ respectively from diameter measurements at each site. Results from the algorithm applied to invasive measurements in paced dogs at a heart rate of 110 beats/min are presented. Figure 1 shows P, $\bar{P}$, p, and u calculated for two measurement sites: the aortic arch and thoracic aorta. Note that the scales for p and u have been adjusted for better comparison. It is important to point out the similarity of $\bar{P}$ in both locations, and the similarity of p and u curves at the

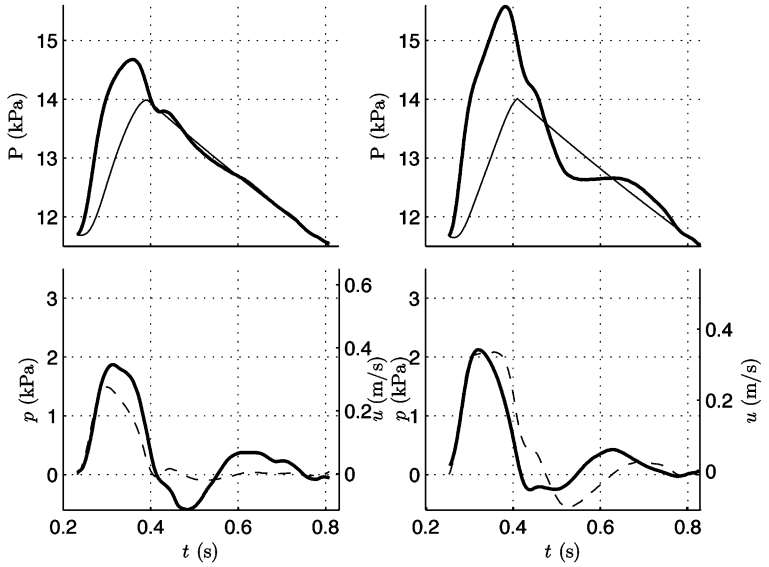

Fig. 1 Measured P (thick curves) and reservoir $\bar{P}$ (thin curves) are shown in the top diagrams and wave pressure p (dashed curves) compared with the wave velocity u (thick curves) are shown in the bottom diagrams The measurements in the aortic arch 11 cm from the aortic valve are shown on the left. The measurements in the thoracic aorta 24 cm from the aortic valve are shown on the right

beginning of systole. Differences between them are due to wave interaction, since they are located at a different distance to main reflection sites. In Fig. 2 the overall set of results are presented and their calculated time constants can be found in the first column of Table 1. The mean and standard deviation of the time constants calculated are $\tau = 2.3 \pm 0.2$ s. All graphs have similar scale ranges to make it easier to observe the contribution of each component to the measured P and U waveforms. $\bar{U}$ generated by $\bar{P}$ is generally low and tends to increase with increasing distance. Note that viscous

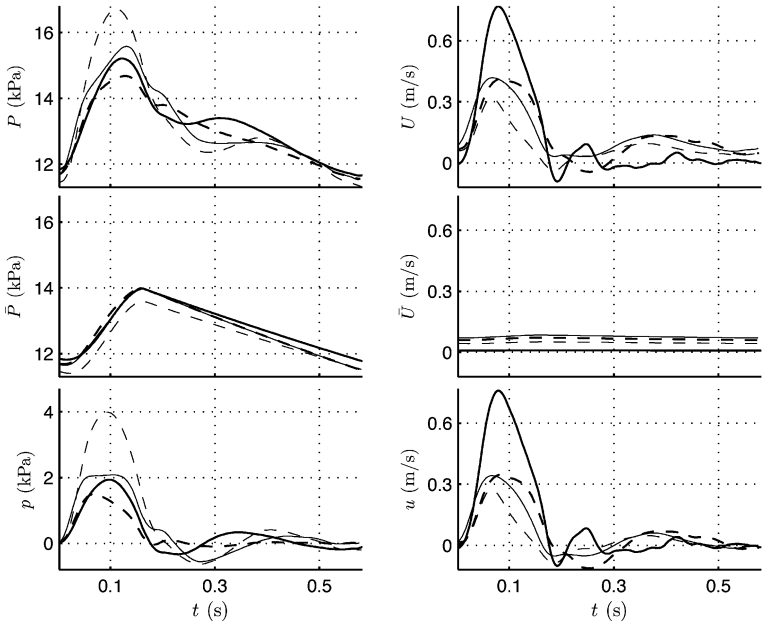

Fig. 2 Simultaneous P and U recordings at four different aortic locations in a dog and their corresponding reservoir–wave separated components, where the pressures are shown on the left, and the velocities on the right: thick solid curves, ascending aorta; thick dashed curves, aortic arch; thin solid lines curves, thoracic aorta; thin dashed curves, abdominal aorta

Table 1 Time constant values τ calculated from simultaneous *in-vivo* pressure measurements in dogs. Three consecutive beats are shown: normal, long, and potentiated (Fig. 7) and paced at different heart rates (Fig. 6). The mean and standard deviation are $\tau = 2.3 \pm 0.2$ s

	τ(s)			
Location	Normal 110 beats/min	Long 110 beats/min	Potentiated 110 beats/min	Normal 60 beats/min
Ascending aorta	2.44	2.50	2.43	2.15
Aortic arch	2.13	2.48	2.03	2.07
Thoracic aorta	2.13	2.58	2.12	2.16
Abdominal aorta	2.52	2.72	2.67	2.37

dissipation accounts for the fall in mean P, mostly noticeable in the reservoir component, while wave activity is responsible for the increase in pulse pressure.

Figure 3 shows the PU-loop from data at the thoracic aorta as suggested by Khir *et al.* [**17**] plus two new curves using the separated components of P and U waveforms. The slope at the beginning of systole corresponds to the wave speed. The pu-loop maintains the same slope as the PU-loop, retaining the wave speed and wave propagation information. Note that the pu-loop was plotted as $p+P_0$ for convenience, with P_0 the measured pressure at the onset of ejection. The wave speed calculated using the slope of the pu-loop at the beginning of systole increases with increasing distance from the aortic valve, indicating the change in the stiffness of the aorta at the different locations measured. The slope of the $\bar{P}\bar{U}$-loop corresponds to $\bar{R}$ which varies at

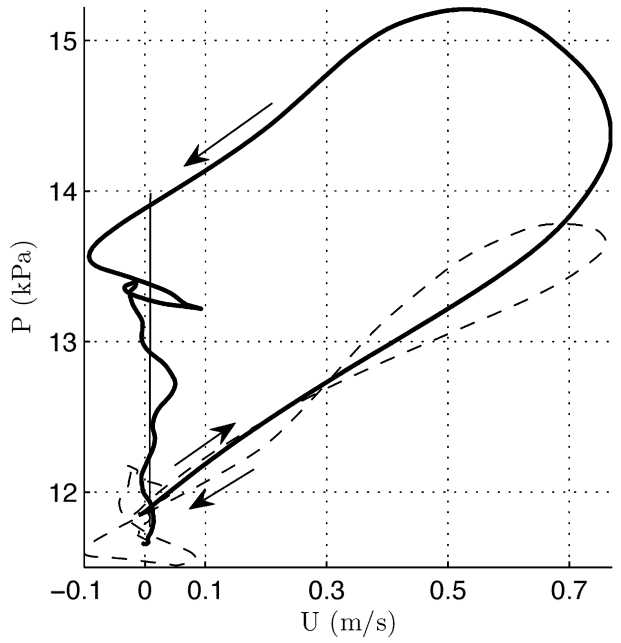

Fig. 3 The PU-loop (thick solid curve), $\bar{P}\bar{U}$-loop (thin solid curve), and pu-loop (thin dashed curve) from the thoracic aorta. Note that $p+P_0$ is used for convenience

different locations because of the distribution of resistances and compliances.

The separation algorithm is also applied to invasive P and U measurements in the descending aorta of human subjects obtained in reference [**14**]. Figure 4 shows the resulting reservoir and wave components of P and U using $P_\infty = 0$. The calculated time constant is $\tau = 1.60$ s.

Figure 5 compares the forward and backward waves obtained using the total P and U measurements in the human descending aorta (curves on the left) against the corresponding values obtained using p and u (curves on the right). Waves are separated using the technique proposed in reference [**7**]. P_0 was subtracted from the data prior to separation for ease of graphical comparison. If the wave separation is performed using P and U, significant wave activity is observed during diastole to produce the exponential decay of P, which consists of self-cancelling waves with equal pressures P_+ and P_- and opposite velocities U_+ and U_- throughout the whole diastolic period. On the other hand, the curves on the right show that the reservoir components $\bar{P}$ and $\bar{U}$ are responsible for the exponential decay of P during diastole. If p and u are used to separate forward- and backward-travelling waves, the resulting p_+, p_-, u_+, and u_- waves are almost zero during diastole, when wave activity is expected to be a minimum. The backward-travelling waves p_- and u_- arrive at mid-systole to produce the characteristic shape of P and U. Note that much of the skewing of U is due to the backward wave u_-; the forward velocity generated by the ventricle is much more symmetrical.

Two of the main advantages of separating the reservoir and wave components from the measured pressure waveform are illustrated in Figs 6 and 7. Figure 6 shows results from separating waves measured in the same experimental dog in the thoracic aorta paced at different heart rates, 110 beats/min on the left and 60 beats/min on the right. Several features of these results are worth noting. The pulse pressure more than doubles as the heart rate is decreased, but most of this difference is due to the

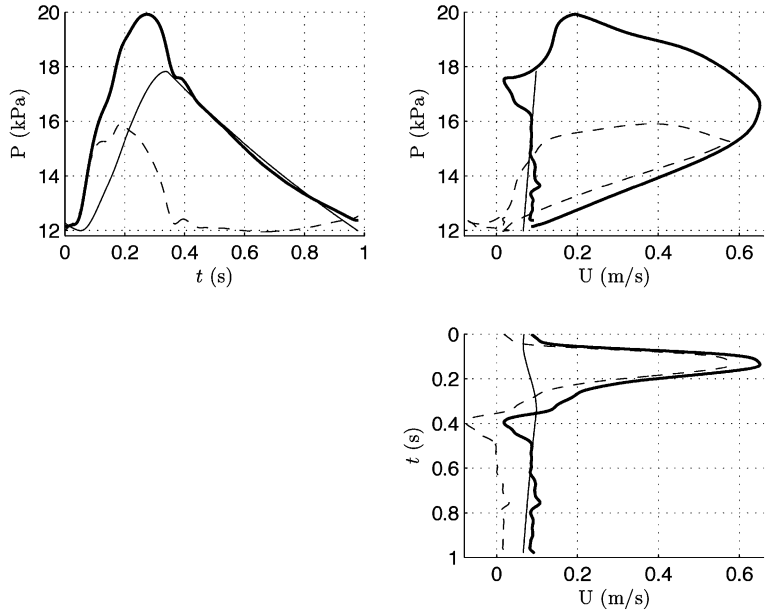

Fig. 4 Reservoir–wave separation in human descending aorta measurements, showing the pressure components P (thick solid curve), $\bar{P}$ (thin solid curve), and p (thin dashed curve), the PU-loop (thick solid curve), $\bar{P}\bar{U}$-loop (thin solid curve), and pu-loop (thin dashed curve), and the velocity components U (thick solid curve), $\bar{U}$ (thin solid curve), and u (thin dashed curve)

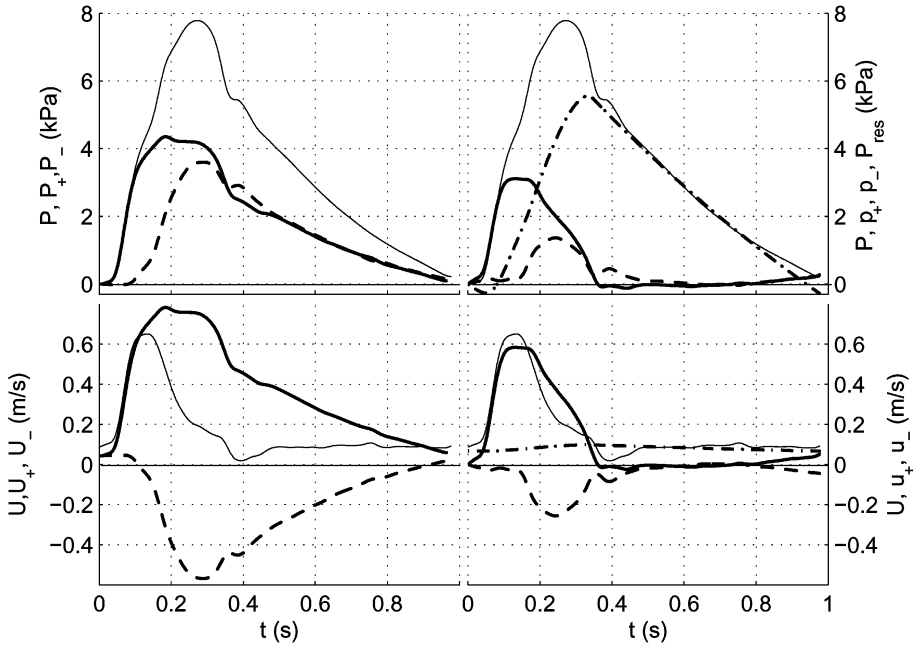

Fig. 5 Wave separation in human descending aorta measurements using the total P and U (on the left) in comparison with wave separation after extraction of $\bar{P}$ and $\bar{U}$ (on the right). Top diagrams: thin solid curves, measured $P - P_0$. Top left diagram: thick solid curve, P_+; thick dashed curve, P_-; note that P_0 was subtracted from P before separation for ease of comparison. Top right diagram: thick dot-dashed curve, $\bar{P} - P_0$; thick solid curve, p_+; thick dashed curve, p_-. Lower diagrams: in thin solid curves, measured U. Lower left diagram: thick solid curve, U_+; thick dashed curve, U_-. Lower right diagram: thick dot-dashed curve, $\bar{U}$; thick solid line curve, U_+; thick dashed curve, u_-. The subscripts + and − indicate forward- and backward-travelling waves respectively with $c = 5.88$ m/s

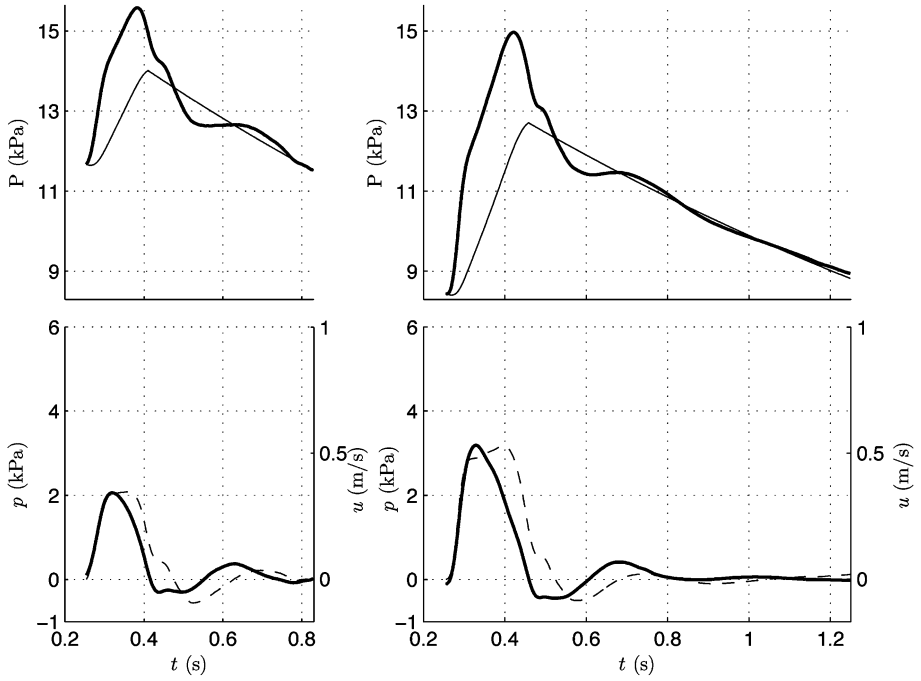

Fig. 6 Reservoir–wave pressure components from the thoracic aorta for the same dog (as shown in Fig. 1) paced at two different heart rates: 110 beats/min (left) and 60 beats/min (right). Measured P (thick curves) and reservoir $\bar{P}$ (thin curves) are shown in the top diagrams and wave pressure p (thin dashed curves) compared with wave velocity u (thick curves) are shown in the lower diagrams

change in the amplitude of the reservoir pressure. The wave pressure component of the measured pressure is remarkably similar at the two heart rates except for an approximately 50 per cent increase in the peak wave pressure at the lower heart rate, consistent with an increased contraction of the ventricle due to an increased filling time according to the Frank–Starling mechanism. It is also noticeable that p and u are similar in shape during the first half of systole and they deviate from each other in a very similar way owing to the arrival of reflected waves. Calculated τ values can be found in the first and fourth columns of Table 1.

Figure 7 shows P, $\bar{P}$, u, p, and the electrocardiogram (ECG) at four simultaneously measured locations of a dog paced at 110 beats/min during a period when an irregularity, a missing beat, occurred. In this case, a normal heart beat is analysed, followed by a long beat caused by the missing beat, subsequently followed by a potentiated beat. These data are rich in content, showing the response at different locations in the arterial tree under normal and irregular conditions. Only a few of the salient features will be mentioned. First, these data show the robustness of the algorithm, which performed convincingly at all locations throughout the period. Second, it should be noted that the reservoir pressures calculated at the different measurement sites are very similar, consistent with the present authors' first hypothesis. Third, the wave pressure in the ascending aorta is very similar in shape to the velocity, as observed in reference [**8**]. This is true during the first part of systole at all sites but, during the latter part of systole, p and u waveforms begin to differ with the differences increasing with increasing distance from the heart. This means that the third assumption becomes progressively worse with increasing distance from the heart valve, where larger reflected waves are expected. Finally, these data are an excellent illustration of the temporal nature of the analysis that enables highly irregular events such as this to be analysed. The time constant τ calculated for each measurement can be found in Table 1.

3.2 Numerical data

The separation algorithm is applied to numerical data obtained using a nonlinear, time-domain, one-dimensional model of pulse wave propagation [**18**, **19**] in a bifurcating network that represents the 37 largest conduit arteries in the human. This numerical model has been validated against a physical representation of the systemic arteries in the human made of silicone tubes [**20**]. With these data, the separation

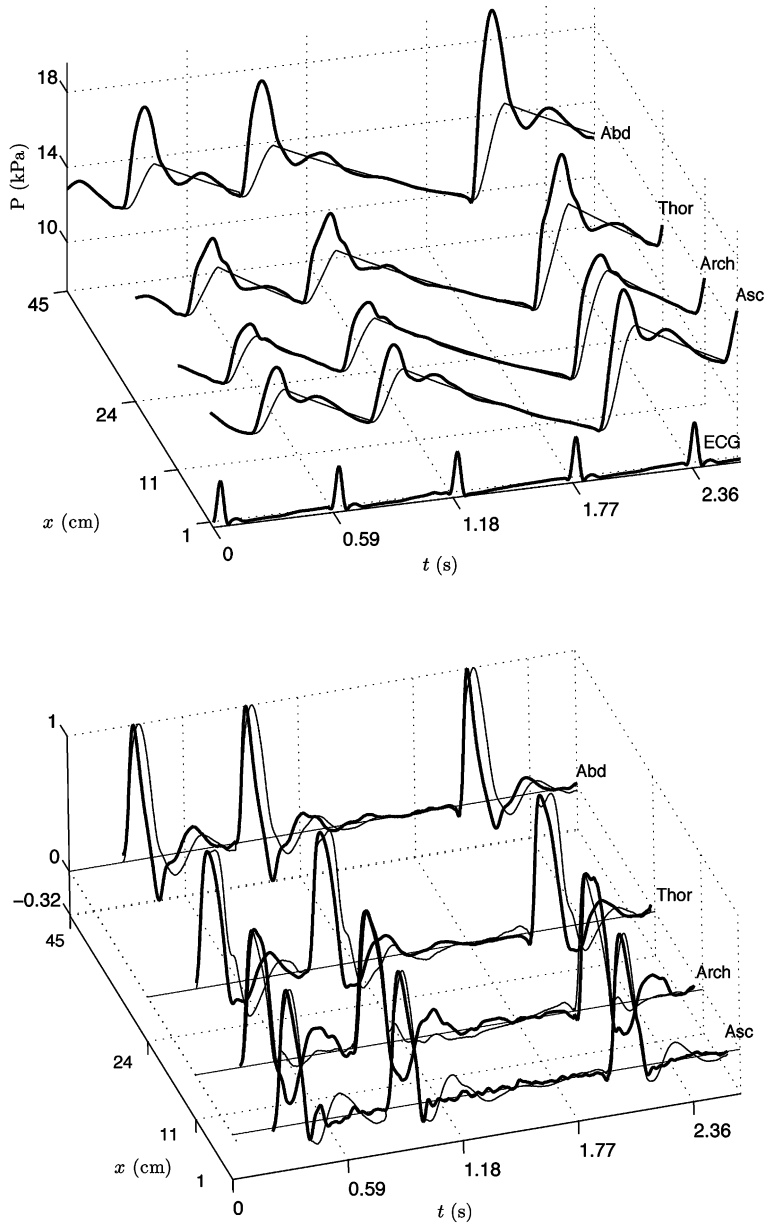

Fig. 7 Three consecutive beats simultaneously measured in four different locations (the abdominal aorta (Abd), the thoracic aorta (Thor), the aortic arch (Arch), and the ascending aorta (Asc) in the aorta of a paced dog at a heart rate of 110 beats/min. Measured P (thick curves) and reservoir $\bar{P}$ (thin curves) are shown in the top diagram and wave p (thin curves) in comparison with wave u (thick curves) in the lower diagram. x refers to the distance from the aortic valve. A normal beat is followed by a long beat and a potentiated beat

technique can be tested not only in the aorta but also in other large arteries, without any measuring error and with an exact knowledge of the total compliance, terminal resistance, and P_∞ of the system.

Figure 8 shows the total pressures simulated by the model and the calculated $\bar{P}$ at four locations along the aorta and at the left brachial and femoral arteries. The following boundary conditions have been considered.

1. The inflow at the ascending aorta is a half-sinusoidal wave during systole followed by a period of reversal flow and zero flow during diastole. Therefore, the assumption $Q_{\text{in}} = 0$ for $T_{\text{N}} \leqslant t \leqslant T$ (see section 2.2) is perfectly satisfied.
2. The total compliance of the system has been increased to 1 ml/mmHg by introducing some peripheral compliance to reduce peripheral wave reflections.

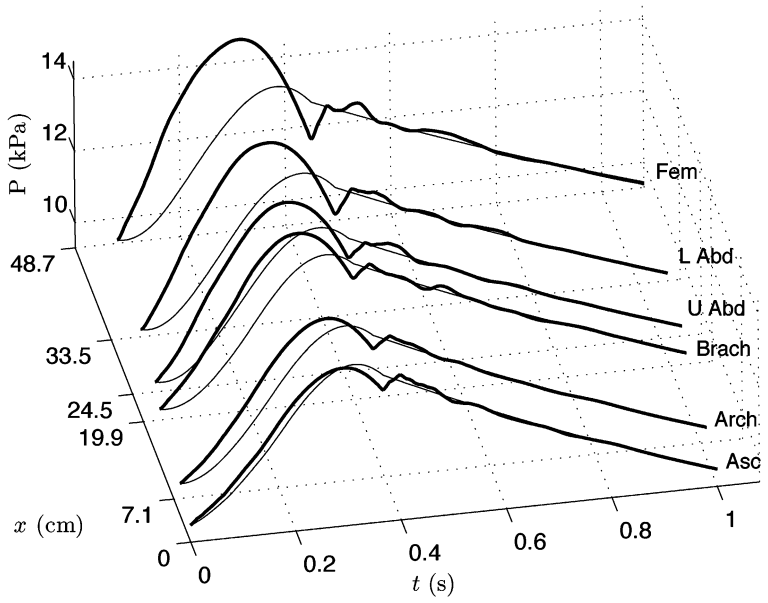

Fig. 8 Total (thick curves) and reservoir (thin curves) pressures at the ascending aorta (Asc), aortic arch (Arch), left brachial (Brach), upper abdominal (U Abd), lower abdominal (L Abd), and left femoral (Fem) arteries simulated using a numerical model containing the 37 largest conduit arteries in humans. x indicates the distance from the inlet of the ascending aorta

3. The cardiac cycle has been increased to 1 s.

Disregarding the time delay of the onset of pressure at different locations, all sites present very similar reservoir pressures (Fig. 9, middle left), which is in accordance with the assumption of a uniform time-varying reservoir pressure in large arteries. Differences arise mainly because of the reduction in mean pressure caused by viscous dissipation. Moreover, reservoir pressures have a larger contribution to the total pressure waveforms than do their wave counterparts (Figure 9, left), which highlights the importance of arterial compliance on pulse wave propagation. On the other hand, reservoir velocities are less significant than their wave components during systole (Fig. 9, right). Reservoir velocities become dominant during diastole. Indeed, wave pressures and velocities are almost zero during diastole, which suggests that wave activity is occurring mainly during systole.

4 DISCUSSION

This work has shown that it is possible to interpret the measured arterial pressure P and velocity U at an arbitrary location in a large artery as the sum of a reservoir components $\bar{P}(t)$ and $\bar{U}(x, t)$ governed by Frank's windkessel model, and the wave components $p(x, t)$ and $u(x, t)$ that vary in time and with distance along the arteries. This separation technique is based on the work by Wang *et al.* at the ascending aorta [**8**] and in the central venous system [**9**]. The present authors have expanded the *ad hoc* ideas of Wang *et al.* to the larger systemic arteries by proposing a separation algorithm that does not require knowledge of the flow into the arterial system. Pressure can be separated into $\bar{P}$ and p from pressure measurements alone at an arbitrary arterial location. In addition, if simultaneous flow measurements are available at the same location, the algorithm used here also allows $\bar{U}$ and u to be determined.

The applicability of the algorithm depends on the extent of validity of the following empirical assumptions: first, the pressure waveform decay behaviour measured at different locations in the arterial system are similar during diastole and, second, the wave component of pressure measured at an arterial location is approximately proportional to the cardiac outflow. In normal subjects, it is believed that both assumptions are valid in large arteries to a first approximation, and they become less valid in distal arterial locations, because reflected waves have a more significant effect on pulse waveforms. Application of the present authors' separation technique to *in vivo* and numerical data has shown the consistency of the two assumptions used by the algorithm, the uniformity of the reservoir pressure in the

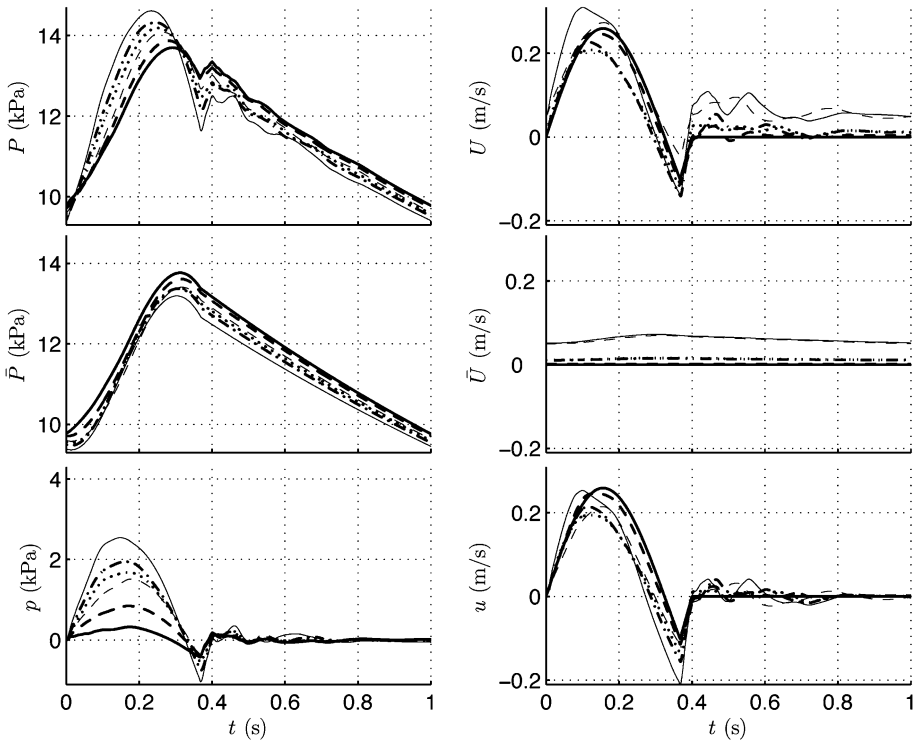

Fig. 9 Total, reservoir, and wave pressures (left) and velocities (right) at the locations shown in Fig. 8, thick solid curves, ascending aorta; thick dashed curves, aortic arch; thin dashed curves, left brachial artery; dotted curves, upper abdominal aorta; thick dot-dashed curves, lower abdominal aorta; thin solid curves, left femoral artery

arterial system, and the close correspondence between the wave pressure and the wave velocity waveforms. The application of the algorithm to the numerically generated data has also shown that the parameters obtained by the fitting process agree well with the known parameters used to generate the data. This increases confidence in the results of the analysis applied to *in vivo* data where the governing parameters are not known.

The method that is proposed is carried out in the time domain and makes no assumption about the periodicity of the data. This is illustrated in the results for the sequence of beats including a missing beat shown in Fig. 7. The algorithm was applied to each beat separately and the calculated time constants τ for each beat are shown in Table 1. The values are reasonably constant at the different locations, which is consistent with the basic assumptions, and for the different beats, which would be expected for the acute nature of the change. The same is true for the difference between normal beats in the same dog with pacing rates of 60 and 110 beats/min, although the heart rate change should be considered more of a chronic than an acute change.

In general, the algorithm cannot be applied to any part of the arterial system or any pathological state in which wave reflections affect the two empirical assumptions significantly. For this reason, the algorithm performs better with a slow heart rate and in arteries close to the ascending aorta. The coronary arteries are a prime example of a region where the algorithm would not be expected to work. Although pressure waveforms in the coronary arteries are very similar to those measured in the aorta of the same subject [**14**], the algorithm cannot be applied to coronary flows because wave activity prevails during all the cardiac cycle, as indicated by the very different velocity waveforms measured in the coronary arteries. The concept of separating the measured pressure into a reservoir pressure and a wave pressure could, however, still be useful in cases such as the coronaries, where the algorithm cannot be used to separate the different pressure contributions. In those cases, it is necessary to have independent knowledge of the flow into the arterial system.

5 CONCLUSIONS

The way in which pressure and flow waveforms measured at an arbitrary location in arteries can be

separated into a reservoir and a wave component has been demonstrated. The model expands and reinforces the work by Wang *et al.* [**8**, **9**], who proposed the wave–reservoir separation of the central aortic pressure provided that the cardiac output is known. The separation technique used here enhances the understanding of the mechanics behind the characteristic shape of the arterial pressure and flow waveforms. Using *in vivo* and numerical data, it has been shown that the largest contribution of the wave components to the total waveforms occurs during the early systolic rise. Later in the cardiac cycle, the reservoir components become dominant. Wave activity is almost non-existent during the last period of diastole. Overall, the reservoir components have a higher contribution to the total waveforms than do the wave components, which highlights the importance of arterial compliance on pulse wave propagation. Wave components are tightly related to the inflow at each heart beat in early systole.

This work has concentrated on the development of an algorithm that would enable the pressure measured at an arbitrary point in the arterial system to be separated into a reservoir pressure and a wave pressure. The demonstration of the utility of this separation remains to be explored fully. Wang *et al.* [**8**, **9**] have explored some of the implications of the separation, but there are many other possibilities. For example, the separation implies that the work done by the left ventricle can be divided into work done to 'fill' the reservoir and the work done to generate the arterial waves. This separation raises interesting possibilities in the interpretation of different physiological and pharmacological interventions. Most of the perfusion of the microcirculation is a result of the reservoir pressure (note that the reservoir velocities tend to increase towards the periphery). The waves, on the other hand, are necessary to generate the reservoir pressure but have little effect on net perfusion.

The effect of the separation on wave intensity analysis also remains to be explored in detail. Figure 3 shows the difference between the *PU*-loop and the *pu*-loop, which could have significant implications for the calculation of the local wave speed from the initial slope of the loop [**17**]. In this particular example, there is only a small difference in slopes, but this may not always be the case. The impact of pressure separation on the sum-of-squares method for calculation of the wave speed has not been studied [**21**]. Since the reservoir pressure is the result of a capacitive-like process, it responds less quickly to the initial compression phase of the left ventricle and so its effect on the wave intensity of the largest waves in the cardiac cycle will be a minimum. For small waves resulting from wave reflections and re-reflections, the effect of subtracting the reservoir pressure from the measured pressure could have a relatively larger effect. This remains to be studied in detail.

ACKNOWLEDGEMENTS

The authors would like to acknowledge Professor John V. Tyberg (University of Calgary) for his support and encouragement. The first author (J. Aguado-Sierra) is supported by the Consejo Nacional de Ciencia y Tecnología de México and the second author (J. Alastruey) by an Engineering and Physical Sciences Research Council Advanced Research Fellowship.

REFERENCES

1 **Frank, O.** Die Grundform des Arteriellen Pulses. *Z. Biologie*, 1899, **37**, 483–526.
2 **Frank, O.** Schätzung des Schlagvolumens des menschlichen Herzens auf Grund der Wellen und Windkesseltheorie. *Z. Biologie*, 1930, **90**, 405–409.
3 **Euler, L.** Principia pro motu sanguinis per arterias determinando. In *Opera posthuma mathematica physica anno 1844 deteclo*, vol. 2 (Eds P. H. Fuss and N. Fuss), 1775, pp. 814–823 (Apund Eggers et Socios, Petropoli).
4 **Riemann, B.** *Gesammelte mathematische Werke und wissenschaftlicher Nachlass*, 1876, pp. 145–164 (B. G. Teubner, Liepzig) (originally published as Uber die Fortpflanzung ebener Luftwellen von endlicher Schwingungsweite. Technical report 8, Göttingen, 1860, 43).
5 **Womersley, J. R.** An elastic tube theory of pulse transmission and oscillatory flow in mammalian arteries. WADC-TR, Technical Report, Wright Air Development Centre, 1957.
6 **Westerhof, N., Elzinga, G.,** and **Sipkema, P.** Forward and backward waves in the arterial system. *Cardiovascular Res.*, 1972, **6**, 648–656.
7 **Parker, K. H.** and **Jones, C. J. H.** Forward and backward running waves in the arteries: analysis using the method of characteristics. *J. Biomech. Engng*, 1990, **11**, 322–326.
8 **Wang, J. J., O'Brien, A. B., Shrive, N. G., Parker, K. H.,** and **Tyberg, J. V.** Time-domain representation of ventricular-arterial coupling as a windkessel and wave system. *Am. J. Physiology, Heart Circulatory Physiology*, 2003, **284**, H1358–H1368.
9 **Wang, J. J., Flewitt, J. A., Shrive, N. G., Parker, K. H.,** and **Tyberg, J. V.** Systemic venous circulation.

Waves propagating on a windkessel: relation of arterial and venous windkessels to systemic vascular resistance. *Am. J. Physiology, Heart Circulatory Physiology*, 2006, **290**, H154–H162.

10 **Westerhof, N., Elzinga, G.,** and **Sipkema, P.** An artificial arterial system for pumping hearts. *J. Appl. Physiology*, 1971, **31**, H776–H781.

11 **Stergiopulos, N., Young, D. F.,** and **Rogge, T. R.** Computer simulation of arterial flow with applications to arterial and aortic stenosis. *J. Biomechanics*, 1992, **25**, 1477–1488.

12 **Lighthill, M. J.** *Waves in fluids*, 1978 (Cambridge University Press, Cambridge).

13 **Alastruey, J., Parker, K. H., Peiró, J., Byrd, S. M.,** and **Sherwin, S. J.** Modelling the circle of Willis to assess the effects of anatomical variations and occlusions on cerebral flows. *J. Biomechanics*, 2007, **40**, 1794–1805.

14 **Davies, J. E., Whinnett, Z. I., Francis, D. P., Manisty, C. H., Aguado-Sierra, J., Willson, K., Foale, R. A., Malik, I. S., Hughes, A. D., Parker, K. H.,** and **Mayet, J.** Evidence of a dominant backward-propagating 'suction' wave responsible for diastolic coronary filling in humans. attenuated in left ventricular hypertrophy. *Circulation*, 2006, **113**, 1768–1778.

15 **Papageorgiou, G. L.** and **Jones, N. B.** Arterial system configuration and wave reflection. *J. Biomed. Engng*, 1987, **9**, 299–301.

16 **Lagarias, J. C., Reeds, J. A., Wright, M. H.,** and **Wright, P. E.** Convergence properties of the Nelder–Mead simplex method in low dimensions. *SIAM J. Optimization*, 1998, **9**, 112–147.

17 **Khir, A. W., O'Brien, A., Gibbs, J. S. R.,** and **Parker, K. H.** Determination of wave speed and wave separation in the arteries. *J. Biomechanics*, 2001, **34**, 1145–1155.

18 **Sherwin, S. J., Franke, V. E., Peiró, J.,** and **Parker, K. H.** One-dimensional modelling of a vascular network in space–time variables. *J. Engng Math.*, 2003, **47**, 217–250.

19 **Alastruey, J.** *Numerical modelling of pulse wave propagation in the cardiovascular system: development, validation and clinical applications*. PhD Thesis, Imperial College London, University of London 2006

20 **Matthys, K. S., Alastruey, J., Peiró, J., Khir, A. W., Segers, P., Verdonck, P. R., Parker, K. H.,** and **Sherwin, S. J.** Pulse wave propagation in a model human arterial network: assessment of 1-D numerical simulations against *in vitro* measurements. *J. Biomechanics*, 2007, **40**, 3476–3486.

21 **Davies, J. E., Whinnett, Z. I., Francis, D. P., Willson, K., Foale, R. A., Malik, I. S., Hughes, A. D., Parker, K. H.,** and **Mayet, J.** Use of simultaneous pressure and velocity measurements to estimate arterial wave speed at a single site in humans. *Am. J. Physiology, Heart Circulatory Physiology*, 2006, **290**, H878–H885.

APPENDIX

Notation

a	γ/C
Abd	abdominal aorta
Arch	aortic arch
Asc	ascending aorta
b	inverse of τ
Brach	brachial artery
c	pulse wave speed
C	compliance of the arterial system
Fem	femoral artery
p	wave pressure
p_+	separated forward-travelling pressure wave using p
p_-	separated backward-travelling pressure wave using p
P	measured pressure
$\bar{P}$	reservoir pressure
P_{in}	pressure at the root of the aorta
P_0	measured pressure at the onset of ejection
$\bar{P}_0$	reservoir pressure at the onset of ejection
P_∞	pressure at which flow in the microcirculation is zero
P_+	separated forward-travelling pressure wave using measured P
P_-	separated backward-travelling pressure wave using measured P
Q_{in}	inflow to the arterial system from the left ventricle
Q_{out}	blood out of the arteries through the microcirculation
R	effective resistance of the peripheral systemic arterial circulation
$\bar{R}$	effective resistance of the vessels downstream of the measurement site
t	time
T	time at which a heart beat ends
Thor	thoracic aorta
T_{N}	time at which the aortic valve shuts at the end of systole
u	wave velocity
u_+	separated forward-travelling velocity wave using u
u_-	separated backward-travelling velocity wave using u
U	measured velocity
$\bar{U}$	reservoir velocity
U_+	separated forward-travelling velocity wave using measured U

U_-	separated backward-travelling velocity wave using measured U
V	volume of the arterial system
x	distance
γ	constant relating Q_{in} and p
ρ	blood density
τ	time constant of the exponential diastolic decay